# Stick-slip behavior in a continuum-granular experiment

Drew A. Geller, Robert E. Ecke, Karin A. Dahmen, and Scott Backhaus

Phys. Rev. E **92**, 060201 — Published 4 December 2015

DOI: 10.1103/PhysRevE.92.060201

# Stick-Slip Behavior in a Continuum-Granular Experiment

Drew Geller,[1] Robert E. Ecke,[1] Karin A. Dahmen,[2] and Scott Backhaus[1]

[1] *Condensed Matter and Thermal Physics Group and Center for Nonlinear Studies Los Alamos National Laboratory, Los Alamos, NM 87545*

[2] *Department of Physics, University of Illinois Urbana Champaign Urbana, Il 61801*

We report moment distribution results from a laboratory experiment, similar in character to an isolated strike-slip earthquake fault, consisting of sheared elastic plates separated by a narrow gap filled with a two dimensional granular medium. Local measurement of strain displacements of the plates at 203 spatial points located adjacent to the gap allows direct determination of the event moments and their spatial and temporal distributions. We show that events consist of spatially-coherent, larger motions and spatially-extended (non-coherent), smaller events. The non-coherent events have a probability distribution of event moment consistent with an $M^{-3/2}$ power law scaling with Poisson-distributed recurrence times. Coherent events have a log-normal moment distribution and mean temporal recurrence. As the applied normal pressure increases, there are more coherent events and their log-normal distribution broadens and shifts to larger average moment.

PACS numbers: 45.70.Ht,46.50.+a,91.30.Px,91.45.cn

Earthquakes involve complex stick-slip motion, heterogeneous material properties, and a large range of length scales from less than a meter to many hundreds of kilometers [1]. One feature of earthquake fault *systems* is a probability distribution of earthquake magnitude $m$ known as the Gutenberg-Richter (GR) law: $\log P(m) \sim -bm$ with $b \approx 1$ [2]. In terms of the moment $M$ released and for globally averaged strike-slip faults (surfaces moving past each other horizontally) the GR distribution is consistent with $P(M) \sim M^{-1-\beta}$ with $\beta \approx 2/3$ [3, 4]. For individual earthquake faults there are examples of GR distributions with a range $0.6 < b < 1.2$ $(0.4 < \beta < 0.8)$ [3–5] and ones where there is a deficit of smaller events and an excess of larger events [6].

Because physical measurements that capture the complexity of real earthquake faults are difficult, theoretical models, laboratory experiments, and numerical simulations have been developed to provide insight into earthquake physics. The simplest ingredients of a strike-slip fault model [1, 7, 8] are continuum elastic plates representing the differential motion of tectonic plates with coupling between the plates determined by frictional interactions. An apparent feature of mature faults is that there is fault gouge—ground up granular matter—at the interface of the plate surfaces [9]. This feature has prompted consideration of the role of idealized granular media subject to compaction and shear in producing stick-slip fluctuations similar in nature to earthquake events [10–15]. Another class of laboratory experiments has focused on effective friction behavior in seismically relevant materials [16] or in block-on-block frictional dynamics [17]. None of these experiments, however, can access the simultaneous spatial and temporal structure of boundary deformations and granular motion, an essential but unstudied aspect of laboratory experimental analogs of earthquake behavior. In our experiment, it is possible to compare individual events in terms of moment, stress change, and gouge kinetics.

Theoretical models incorporate various ingredients from continuum properties [1] to statistical physics approaches [7, 8] that include discrete granular interactions. These models are usually studied using numerical simulations [1, 7, 8, 18–20] but some models are amenable to analytical calculation and predict universal scaling behavior in the limit of long-range forces, i.e., in the mean field limit [21, 22]. Universal models are compelling in that they do not rely on detailed modeling of all the relevant physics of earthquakes and other stick-slip systems. The major predictions for mean field theory models [21–23] concern the slip moment $M$ which is the sum of the individual local displacements $s$ induced in an event. These local displacements are spatially distributed along the slip plane as in real earthquakes. The probability distribution $P(M)$ is predicted to scale as $M^{-3/2}$ for small $M$ (the -3/2 power law is within the range -1.4 to -1.8 exponents observed in real earthquakes) whereas there may be enhanced probability for large moment events if there is frictional weakening.

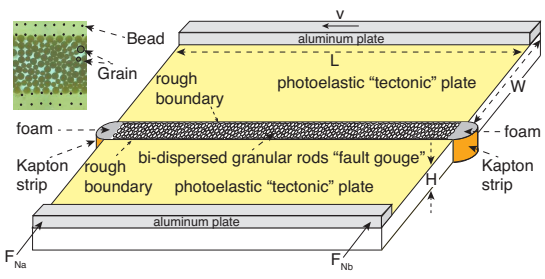


FIG. 1. (Color online) Schematic illustration of experimental laboratory earthquake apparatus

We have developed a laboratory analog of a single strike-slip fault with continuum plates and granular fault gouge that uniquely allows the determination of the spatial and temporal properties of both the elastic plate de-

formations and the microscopic motion of the granular material. We measure the local slip $s$ and the total slip moment $M$ associated with stick-slip events that occur as the system is slowly sheared. The spatial structure of the slip events along this fault is directly observed in contrast to other experiments of this class [15, 16]. The experiment has two soft plates, one fixed and the other sheared at fixed velocity, and the forces between the plates are coupled across a narrow gap by a confined quasi two-dimensional granular material. We find that the total probability distribution of $M$ is consistent with the mean-field prediction [21, 22] of $M^{-3/2}$ for small $M$ but shows a crossover to a surplus of large moment events as the applied normal pressure $P_N$ is increased. When the events are divided into "coherent" (C), large, spatially localized ones and smaller, less spatially localized, "non-coherent" (NC) events, the NC probability distribution is well described by a $M^{-3/2}$ distribution over about two decades in $M$ and the mean-recurrence time distribution is a decaying exponential, i.e., a Poisson process, consistent with predictions of mean field theory [21, 23]. The probability distribution of C events is broadly peaked, consistent with a log-normal distribution whose peak shifts towards higher moment and broadens with increasing normal force. There is a mean recurrence time for C events which increases with increasing $P_N$. Our measurements strongly demonstrate the emergence of the two types of earthquake behaviors observed in nature [6] in a *single* fault of coupled continuum plates and granular fault gouge, where the role of the granular stress chains is to induce dynamical spatial heterogeneity of force distributions.

Our experimental apparatus, see Fig. 1, consists of two plates formed from photo-elastic material (Vishay PS-4) with dimensions $L = 50$ cm, $W = 25$ cm, and $H = 1$ cm. The plate material has an elastic modulus $E_p = 2.5$ MPa and a Poisson ratio of 0.50. Aluminum supports on the outer edges provide structural support and are respectively sheared at one boundary using a linear translation stage driven by a stepper motor while compressed by a normal force $F_N$ in the range $20 < F_N < 200$ N applied to the fixed boundary at the start of the run. We define a dimensionless normal pressure as $P_N = F_N/(LHE_p)$.

The plates are spaced $W_g \approx 1$ cm apart and the gap is filled with a bi-dispersed set of $N_g = 3000$ nylon rods with height H and diameters 0.119 and 0.159 cm aligned parallel to one another. The elastic modulus of the granular rods is $E_g \approx 4$ GPa, much stiffer than the plate material (a more realistic earthquake situation would be $E_p \approx E_g$). At both ends of the gap, a plastic strip confines the granular material, and a piece of foam keeps the force more or less constant as the plates translate. The total physical displacement in an experiment is $\pm 2$ cm corresponding to total strain of about 0.04 ($\Delta x/L$), and the shearing velocity $v \approx 4$ $\mu$m/s corresponds to a strain rate $\dot{\gamma}_H = v/W_g = 4 \times 10^{-4}$/s (or based on $L$: $\dot{\gamma}_L = v/L = 8 \times 10^{-6}$/s). The strain rate gives a time scale $\tau_H = 1/\dot{\gamma}_H = 2500$ s.

The boundary conditions between the elastic plates and the granular packing are mediated by a regularly spaced array of 202 of the larger diameter nylon rods glued into each of the elastic plates at the edge of the fault. Additionally, 812 (4 rows of $N_p = 203$) ball bearings of 300 $\mu$m diameter are fixed in two rows on the top surface of each plate near the inner edge with nominal $\ell = 0.22$ cm separation, as can be seen in the detailed view in the upper left hand corner of Fig. 1. These ball bearings do not contact the granular gouge but instead serve as fiducial markers, showing the local displacements of the elastic plate (here we use one row on the fixed plate and one on the moving plate). Photographic digital images ($3024 \times 4032$ pixels) of the ball bearings are taken every $\delta t = 2.5$ sec (500 motor steps) and provide individual locations $\{x_i, y_i\}^j$ with relative error of $\delta = 12$ $\mu$m (0.2 pixels) where $i$ labels the distance along the gap, and $j$ is the time index in units of $\delta t$. As the plates are sheared, the bead arrays deform to follow the elastic response of the plates. The differential motion between successive time steps of bead $i$ is defined as $s_i^j = \left(x_i^j - x_i^{j-1}\right) \theta\left(x_i^j - x_i^{j-1} - \delta_n\right)$ where $\delta_n = 1.5\delta$ and $\theta(x)$ is the Heaviside function; values below our noise threshold are set to zero and we define the number of non-zero contributions $N^j = \sum_{i=1}^{N_p} \theta(s_i^j - \delta_n)$. The spatially-integrated moment at time step $j$ is $m^j = \sum_{i=1}^{N_p} s_i^j$, and the dimensionless moment for the event at time $j$ is $M^j = m^j \alpha \ell H/(H^2 \ell) = m^j \alpha/H$ where $\alpha = 60$ $\mu$m/pixel is a calibration factor.

One unique aspect of our experiments is the ability to determine the spatial distribution of stick-slip events. In Fig. 2(a), we show a typical set of displacements $s_i$ versus normalized time $t/\tau_H$ for lateral positions $x/L = 1/4$, $1/2$, and $3/4$. Large displacements indicated by dashed lines occur over the whole fault length whereas the spatial coherence of smaller events varies. A more indicative representation of spatial coherence can be seen in a space-time plot of the magnitude of differential displacements in Fig. 2(b). Large, fault-spanning events (solid vertical lines spanning most of $L$ in Figs. 2(b),(c)) occur frequently for these conditions (the frequency increases and the events become more nearly periodic at higher $P_N$). A close-up view of the motions near the center of the fault in Fig. 2(c), shows detail of smaller events in which only a few locations or clusters of beads slip in a given time interval.

In addition to global events and spatially extended ones, there are spatially localized events that have length less than $L$. This variation arises from the heterogeneous force distribution in the granular material set up by stress chains. To extract more detailed spatial information, the center for an event at time $j$ is defined by the displacement-weighted bead position $X^j = \left(\sum_{i=1}^{N_p} s_i^j x_i^0\right)/M^j$, where $x_i^0$ is the nominal initial position of the bead $i$. The spatial extent of event $j$ is proportional to the radius of gyration,

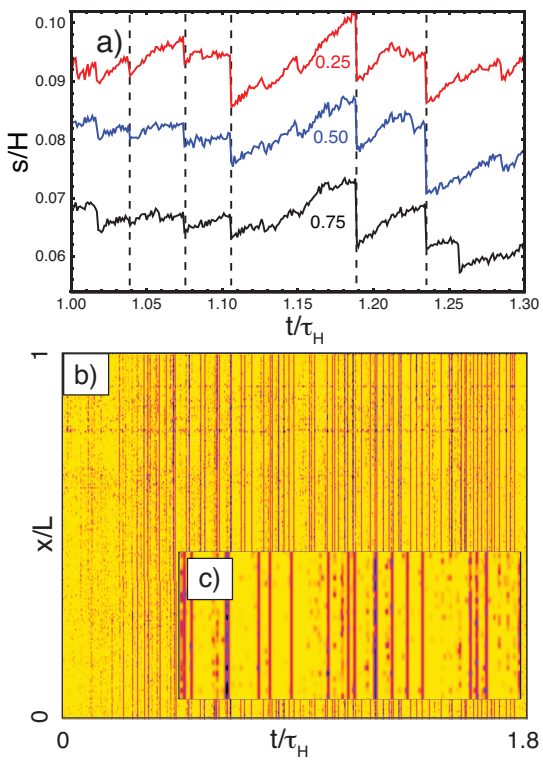


FIG. 2. (Color online) (a) Typical $s/H$ vs $t/\tau_H$ for $x/L = 1/4,\ 1/2$, and $3/4$; $P_N = 4.8 \times 10^{-3}$. (b) The space-time displacements of beads indicated by intensity where darker points indicate more motion; $P_N = 6.4 \times 10^{-3}$. The ordinate is $x/L$ and normalized time $t/\tau_H$ proceeds from left to right. The system reaches steady state for $t/\tau_H > 0.4$, roughly independent of $P_N$. (c) Expanded segment of space-time plot in b).

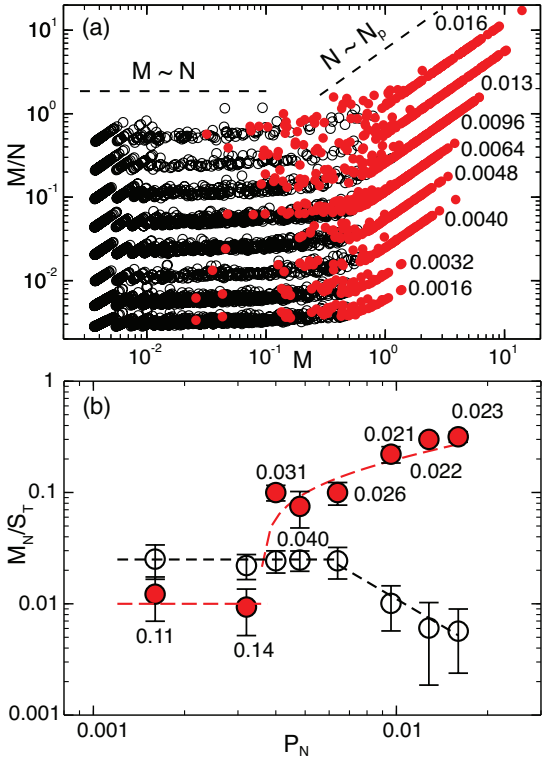


FIG. 3. (Color online) (a) Average slip M/N vs. M for labeled $P_N$. Curves are offset vertically for clarity (coherent: solid red; non-coherent: open black). (b) Fraction of moment $M_N$ relative to available total strain moment $S_T$ (coherent: solid red; non-coherent: open black). Dashed lines - see text. The mean recurrence times for C events are labeled.

$R^j = \left(\sum_{i=1}^{N_p} s_i^j \left(X^j - x_i^0\right)^2 / M^j\right)^{1/2}$. A related normalized quantity that reflects the spatial coherence of an event: $C^j = R^j/(\sqrt{12}N^j)$ (the numerical factor gives $C^j = 1$ for a spatially uniform event of any extent with constant amplitude).

For most events, typically involving motion at a small number of locations, $M/N$ (each data point denotes an event with $M^j$ and $N^j$) is nearly constant as a function of $M$, as seen in Fig. 3(a). The average motion typically spans a small range, so that events differ in moment owing to the number of beads $N^j$ involved rather than the distance that they move. For high moments, $M/N$ is linear in $M$ because the number of beads participating in a slip event is limited by the size of our experiment, i.e., $N^j \approx N_p$ so that $M/N$ can only grow in proportion to the average bead displacement. These events achieve much higher average displacements per bead than the spatially localized events because no locations remain pinned by force chains across the gouge. This behavior suggests that events can be divided into two populations: C are system spanning events and NC as smaller events (see also [15]). We refine this division by including as coherent events spatially localized ones with $C^j < 2$ and where $M^j/N^j > 0.003$ $(2.5\delta/H)$; the latter criterion is a minor one. Our results do not depend sensitively on either cutoff. Both types of events are indicated in Fig. 3(a).

For any particular shear experiment, the system reaches a steady state after a "run-in" period $T_r \approx 0.4\tau_H$. In the steady state the system is essentially in the plastic yield limit, such that the fixed plate no longer has a time-averaged motion accumulating elastic energy. The shear imparted by the moving plate must be released over time, and we quantify the stick-slip versus sliding contributions to this motion by comparing the total event moment per site $M_N = (1/N_p)\sum_{j:\ T_j > T_r} M^j$ to the total displacement of the moving plate $S_T = v(T_f - T_r)$ for the remainder of the experiment (of total duration $T_f$) after run-in. To improve the statistics of the measurement, several runs at nearly the same conditions (the configuration of stress chains and gouge particles will differ, but $P_N$ can be held approximately constant) are combined in calculating $M_N$ and $S_T$.

Figure 3(b) shows that $M_N$ of all C and NC events recorded for the fixed plate captures less than 30% of the continual motion of the driven plate over the full range of normal pressure studied. The contribution of the C

events increases dramatically in the range $P_N > 0.0036$ consistent with $(P_N - 0.0036)^{1/2}$ (long dashed curve in Fig. 3(b) for $P_N > 0.0036$ ), perhaps indicative of a bifurcation, and the contribution of these events is larger than that for NC events except at very low $P_N$. The NC events account for a constant fraction of the motion up to $P_N \approx 0.0064$, above which their contribution declines rapidly. The remaining ($> 70\%$) fraction of the available motion results from steady sliding (integrating M P(M) for events below the noise threshold yields a contribution of less than 10% to the total moment). In MF models of stick-slip behavior [21, 24], sliding does not affect the expected scalings. This measurement has analogy in the seismic coupling (ratio of seismic slip to total slip) of real earthquake faults with values less than 1 observed, for example, for creeping regions of the San Andreas fault and for many subduction faults [25].

The probability distribution of event moments for different $0.0016 < P_N < 0.016$ is shown in Fig. 4(a). As $P_N$ increases, the probability of NC events decreases, consistent with trends in models [22] that include the effects of packing fraction $\phi$ ($\phi$ increases slightly with increasing $P_N$). The large C events become more probable, growing at the expense of the NC events, and have higher mean $M$ for larger $P_N$. Using the decomposition into C and NC events, we represent their individual contributions to the overall probability distribution $P(M)$. In Fig. 4 (b), we show the NC distribution (normalized to the number of NC events) and in the inset Fig. 4 (b) we show the C distribution and its variation with $P_N$. This decomposition demonstrates that NC events are distributed as a power law over about 2 decades in M consistent with $M^{-3/2}$ (the remaining depletion/enhancement of $M$ may be a finite size effect). On the other hand, the C events are concentrated at large $M$ with broader distribution and higher mean $M$ as $P_N$ increases. Once one divides out the C events, the resultant PDFs are consistent with log-normal distributions of the form: $P(M) = \left(1/\left(x\sigma\sqrt{2\pi}\right)\right) e^{-(\log x - \mu)^2/\left(2\sigma^2\right)}$. We fit the probability distributions to this form. The fitted values of $\mu$ and $\sigma$ for the curves shown in the inset of Fig. 4: $\{0.0016 \leq P_N \leq 0.004, -0.4, 0.45\}$, $\{0.0048 \leq P_N \leq 0.0064 : 0.24, 0.6\}$, and $\{0.0096 \leq P_N \leq 0.016 : 1.0, 1.2\}$. The mean moment of C events grows with increasing $P_N$ as does the range of moment sizes as reflected in the standard deviation of the distribution.

In addition to the excess large-event probability at higher $P_N$, the C events develop a dominant mean repetition time $\tau$ for large $P_N$, see Fig. 2(b),(c). In contrast, the NC events are consistent with an exponential distribution in $\tau$, representative of a Poisson process. For C events, the mean repetition time is $0.02 < \tau/\tau_H < 0.04$ with small overall variation with $P_N$ (values labeled for data points in Fig. 3(b)). Many laboratory based experiments and model simulations show the emergence of a mean repetition time associated with large brittle events [1, 21, 22].

The probability distribution of event moments can be

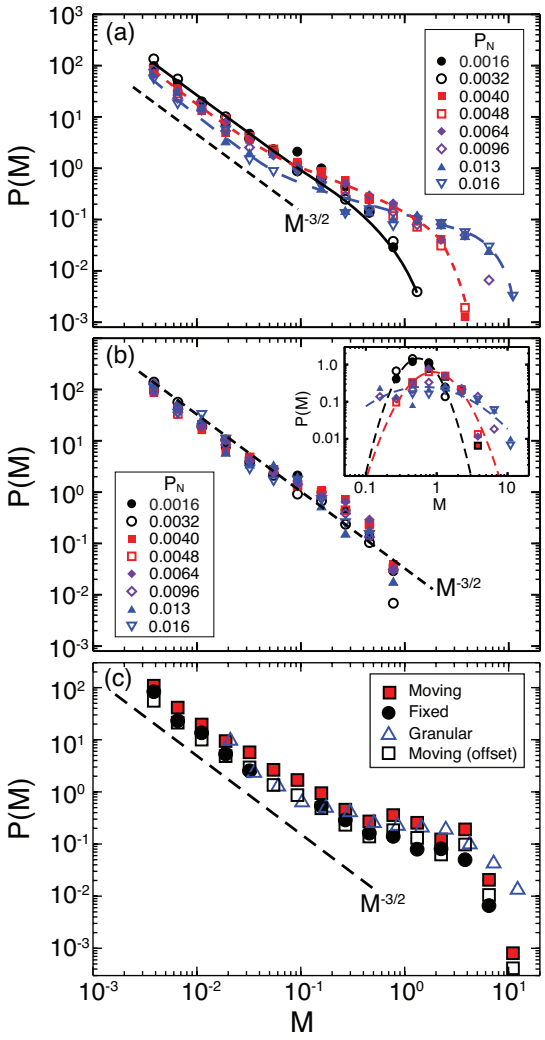


FIG. 4. (Color online)$P(M)$ vs $M$ for different $P_N$: (a) All events; (b) NC events and inset: C events; (c) All events for $P_N = 9.6 \times 10^{-3}$ measured on moving boundary (solid square; open square offsets M for comparison), fixed boundary (solid circles), and for granular displacements $M_g$. Solid, short-dashed and long-dashed curves are guides to the eye for different $P_N$. The dashed lines in inset of (b) are fits to log-normal distributions. $M^{-3/2}$ scaling labeled by (black) dashed line in (a) and (b).

determined in various ways from experimental measurements. As described above, one can evaluate the moment event distribution measured for the fixed plate. After an initial transient, the mean total displacement of the fixed plate is zero, i.e., the plate has no mean translational motion. Data for $P_N = 0.0096$ from fixed plate measurements are shown in Fig. 4(c). For comparison, we also show data for the moving plate which is evaluated along the moving side of the gap after subtracting the mean translational velocity. There is a slight difference in amplitude of the response but the dependence on $M$ is almost identical to that of the fixed plate. Fi-

nally, we measure the positions $\mathbf{r}_i^j$ of $N_g$ particles in the fault gap where $j$ indexes the time increment and the index $i$ labels each particle. The differential displacements $\Delta\mathbf{r}_i^j = \mathbf{r}_i^j - \mathbf{r}_i^{j+1}$ are determined and the total squared displacements $M_g^2 = \sum_{i=1}^{N_g}\left((\Delta x_i)^2 + (\Delta y_i)^2\right)$ offers another quantitative measure of the event moment. In Fig. 4(c), one sees that the scaling for granular displacements $M_g$ is very similar to those obtained from the fixed and moving plates where we have adjusted the magnitude for the different numbers of elements involved, i.e., roughly by the ratio $N_g/N_p$. From this comparison of scaling behavior using different measures of motion for slip events, we conclude that the scaling we observe is a robust feature of our experimental system and not limited to slip events on the fixed plate.

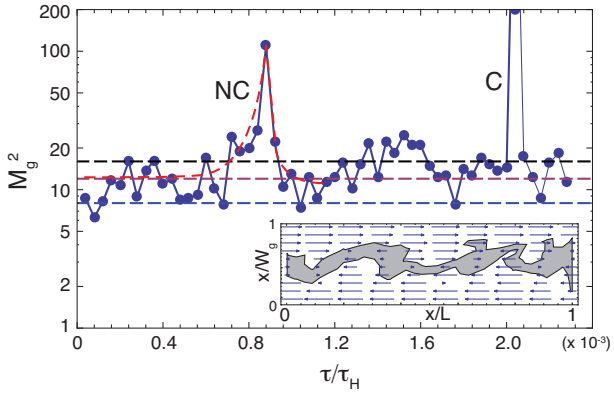


FIG. 5. (Color online) (a) Total granular squared displacement magnitude $M_g^2$ (background noise subtracted) vs $\tau/\tau_H$; a C ($M_g^2 \sim 10^4$) and a NC event are labeled ($P_N = 0.0096$). Horizontal lines show mean and plus/minus one standard deviation of noise. Inset shows spatial average (on a $10 \times 10$ grid) of lateral displacements of granular particles over the central third of the fault in a C event showing irregular shear localization (shaded contour).

Earthquake motion is sometimes described as an effective brittle fracture and analogies drawn with the fracture of heterogenous rock samples [26]. C events in our system have much in common with brittle fracture [27, 28]: 1) yield force for C events increases roughly linearly with $P_N$; 2) average mean displacement of fixed plate (proportional to $P_N$) shows no pre-event plastic deformation, i.e., the stress-strain curve is typically linear up to the C event; 3) no measurable precursor signature for a C event in the microscopic granular mean-square displacement signal whereas NC events may show some pre-event and post-event signature, see Fig. 5; 4) shear localization on the scale of several bead diameters for C events, inset of Fig. 5, in which the motion shown is heterogeneous over the central third of the fault section but the majority of the shear motion is concentrated in a vertically localized section of width 1 to 2 grain diameters as indicated by the shaded region. In many features, C events are similar to Mode II fracture [28]. The direct correspondence between brittle fracture of a cohesive material and the formation of strain localization in a sheared, compressed granular media is incomplete but the similarities suggest that a characterization of large C events as "brittle" is not unreasonable.

The moment distribution scaling for NC events with the emergence of C events combined with the concurrent development of a mean recurrence time $\tau/\tau_H \approx 0.025$ and the demonstrated spatial coherence of C events with increasing $P_N$ gives a cohesive picture of system behavior. At small normal force, spatial and temporal correlations are weak giving rise to random spatially extended events and power law $M^{-3/2}$ scaling corresponding to the "fluid"-like phase in mean field theory [22]. As $P_N$ increases, the granular media compacts owing to compressive stresses and more effectively couples motion on either side of the gap. This coupling leads to a larger fractional moment slipped, a mean recurrence time between events, and many more spatially compact events with $R^j \sim L$. Our results are consistent with a system having frictional weakening.

The full physical picture of the phenomena we report is complex involving the rheology of the sheared granular medium. Many other features of the experimental data are possible including a "microscopic" elucidation of the individual motions of the grains and their individual or collective motion in events [14]. Finally, our results have qualitative representation in the behavior of individual earthquake faults. For example, brittle strength increases with depth, and the largest earthquakes are nucleated near the base of the seismogenic zone [25], consistent with our observations of increased likelihood of large events at higher normal pressure.

We acknowledge conversations with Karen Daniels and Jonathan Uhl. Work at Los Alamos National Laboratory was funded by the LDRD program under the National Nuclear Security Administration of the U.S. Department of Energy under Contract No. DE-AC52-06NA25396. K.D. acknowledges support from grants NSF DMR 1005209 and NSF DMS 1069224.

[1] Y. Ben-Zion, Reviews of Geophysics **46**, 1 (2008).
[2] B. Gutenberg and C. F. Richter, Annals of Geophysics **9**, 1 (1956).
[3] C. Frohlich and S. Davis, Journal of Geophysical Research **98**, 631 (1993).
[4] Y. Y. Kagan, Geophysical Journal International **148**, 520 (2002).
[5] D. Schorlemmer, S. Weimer, and M. Wyss, Nature **437**, 539 (2005).
[6] M. W. Stirling, S. G. Wesnouskey, and K. Shimazaki, Geophysical Journal International **124** (1996).
[7] J. M. Carlson, J. S. Langer, and B. E. Shaw, Reviews of Modern Physics **66**, 657 (1994).
[8] H. Kawamura, T. Hatano, N. Kato, S. Biswas, and B. K. Chakrabarti, Reviews of Modern Physics **84**, 839 (2012).
[9] F. Chester and J. Chester, Tectnophysics **295**, 199 (1998).
[10] D. Howell, R. P. Behringer, and C. Veje, Physical Review Letters **82**, 5241 (1999).
[11] L. Bocquet, W. Losert, D. Schalk, T. C. Lubensky, and J. P. Gollub, Physical Review E **65**, 011307 (2001).
[12] D. Fenistein and M. van Hecke, Nature **425**, 256 (2003).
[13] T. S. Majmudar and R. P. Behringer, Nature **435**, 1079 (2005).
[14] K. E. Daniels and N. W. Hayman, Journal of Geophysical Research-Solid Earth **113**, B11411 (2008).
[15] N. W. Hayman, L. Ducloué, K. L. Foco, and K. E. Daniels, Pure and Applied Geophysics **168** (2011).
[16] C. Marone, Annual Review of Earth and Planetary Sciences **26**, 643 (1998).
[17] O. Ben-David, G. Cohen, and J. Fineberg, Science **330**, 211 (2010).
[18] J. I. Katz, Journal of Geophysical Research **91**, 10412 (1986).
[19] J. B. Rundle, D. L. Turcotte, R. Shcherbakov, W. Klein, and C. Sammis, Reviews of Geophysics **41**, 1019 (2003).
[20] M. P. Ciamarra, E. Lippiello, C. Godano, and L. de Arcangelis, Physical Review Letters **104** (2010).
[21] D. S. Fisher, K. Dahmen, S. Ramanathan, and Y. Ben-Zion, Physical Review Letters **78**, 4885 (1997).
[22] K. A. Dahmen, Y. Ben-Zion, and J. T. Uhl, Nature Physics **7**, 554 (2011).
[23] K. A. Dahmen, Y. Ben-Zion, and J. T. Uhl, Physical Review Letters **102** (2009).
[24] M. LeBlanc, L. Angheluta, K. Dahmen, and N. Goldenfeld, Physical Review E **87**, 022126 (2013).
[25] C. H. Scholz, *The Mechanics of Earthquakes and Faulting* (Cambridge University Press, Cambridge, UK, 2002).
[26] K. Mogi, Bulletin of the Earthquake Research Institute **40**, 125 (1962).
[27] M. J. Alava, P. K. V. V. Nukala, and S. Zapperi, Advances in Physics **55**, 349 (2006).
[28] B. R. Lawn, *Fracture of Brittle Solids*, Solid State Science (Cambridge University Press, Cambridge, UK, 1993), 2nd ed.